Since January 2020 Elsevier has created a COVID-19 resource centre with free information in English and Mandarin on the novel coronavirus COVID-19. The COVID-19 resource centre is hosted on Elsevier Connect, the company's public news and information website.

Biosensors and Bioelectronics 205 (2022) 114094

Contents lists available at ScienceDirect

Biosensors and Bioelectronics

journal homepage: www.elsevier.com/locate/bios

Plasmon color-preserved gold nanoparticle clusters for high sensitivity detection of SARS-CoV-2 based on lateral flow immunoassay

Hyun-Kyung Oh [a,b,1], Kihyeun Kim [a,c,1], Jinhee Park [d], Hyungsoon Im [c,e], Simon Maher [b], Min-Gon Kim [a,d,*]

[a] Department of Chemistry, Gwangju Institute of Science and Technology (GIST), Gwangju, 61005, Republic of Korea
[b] Department of Electrical Engineering and Electronics, University of Liverpool, Brownlow Hill, Liverpool, L69 3GJ, UK
[c] Center for Systems Biology, Massachusetts General Hospital, Boston, MA, 02114, USA
[d] GMD BIOTECH, INC, Gwangju, 61005, Republic of Korea
[e] Department of Radiology, Massachusetts General Hospital, Boston, MA, 02114, USA

ARTICLE INFO

Keywords:
Gold nanoparticle cluster
Plasmonic
Lateral flow immunoassay
SARS-CoV-2
Colorimetric sensor
COVID-19

ABSTRACT

Lateral flow immunoassays (LFI) have shown great promise for point-of-care (POC) sensing applications, however, its clinical translation is often hindered by insufficient sensitivity for early detection of diseases, including severe acute respiratory syndrome coronavirus 2 (SARS-CoV-2). This is mainly due to weak absorption signals of single gold nanoparticles (AuNPs). Here, we developed AuNP clusters that maintain the red color of isolated individual AuNPs, but increase the colorimetric readout to improve the detection sensitivity. The plasmon color-preserved (PLASCOP) AuNP clusters is simply made by mixing streptavidin-coated AuNP core with satellite AuNPs coated with biotinylated antibodies. The biotinylated antibody-streptavidin linker forms a gap size over 15 nm to avoid plasmon coupling between AuNPs, thus maintaining the plasmonic color while increasing the overall light absorption. LFI sensing using PLASCOP AuNP clusters composed of 40 nm AuNPs showed a high detection sensitivity for SARS-CoV-2 nucleocapsid proteins with a limit of detection (LOD) of 0.038 ng mL^{-1}, which was 23.8- and 5.9-times lower value than that of single 15 nm and 40 nm AuNP conjugates, respectively. The PLASCOP AuNP clusters-based LFI sensing also shows good specificity for SARS-CoV-2 nucleocapsid proteins from other influenza and coronaviruses. In a clinical feasibility test, we demonstrated that SARS-CoV-2 particles spiked in human saliva could be detected with an LOD of 54 $TCID_{50}$ mL^{-1}. The developed PLASCOP AuNP clusters are promising colorimetric sensing reporters that present improved sensitivity in LFI sensing for broad POC sensing applications beyond SARS-CoV-2 detection.

1. Introduction

The worldwide COVID-19 pandemic has increased the urgency for point-of-care (POC) testing, which can inform a preliminary test result at the point of need (Drain et al., 2014; Price, 2001; Vashist et al., 2015; Warsinke, 2009). Among various POC schemes presented, colorimetric lateral flow immunoassay (LFI) has become one of the most favorable methods because the test is cheap, fast, simple, and easy to use, which can be detected by the naked-eye without an additional detection system (Koczula and Gallotta, 2016; Sajid et al., 2015; Wang et al., 2016). Many LFI platforms use 20–60 nm gold nanoparticles (AuNPs) as colorimetric detection probes. AuNPs have strong visible light absorption induced by localized surface plasmon resonance (LSPR), allowing for naked-eye detection (Parolo et al., 2020; Zhou et al., 2015). Moreover, the surface of AuNPs can be readily functionalized with antibodies for specific target molecules (Parolo et al., 2020). These properties make AuNPs highly suitable for colorimetric LFI sensing to enable rapid testing (Zhang et al., 2020b).

While AuNP-based LFI testing is widely applicable for POC testing, it often suffers from a low sensitivity (Diaz-Gonzalez and de la Escosura-Muniz, 2021). There have been attempts to improve the sensitivity by enhancing colorimetric signals using larger AuNPs or AuNP clusters exhibiting higher optical absorption (Chen et al., 2020; Khlebtsov et al., 2019; Li et al., 2016; Shen and Shen, 2019; Shirshahi

* Corresponding author. Department of Chemistry, Gwangju Institute of Science and Technology (GIST), Gwangju, 61005, Republic of Korea.
E-mail address: mkim@gist.ac.kr (M.-G. Kim).
[1] These authors contributed equally to this work.

https://doi.org/10.1016/j.bios.2022.114094
Received 10 November 2021; Received in revised form 30 January 2022; Accepted 10 February 2022
Available online 17 February 2022

and Liu, 2021). For example, Juan et al. reported that the use of 100-nm AuNPs for LFI showed 5.3 times higher sensitivity than that of 20-nm AuNPs (Li et al., 2016). However, increasing the size of AuNPs over 100 nm does not further enhance the sensitivity due to the light absorption leveling off above 100 nm and the low diffusivity (Chen et al., 2020). Alternatively, the light absorption can be increased by forming AuNP clusters, because the light absorption intensity increases in accordance with the number of AuNPs that form a cluster.

While forming AuNP clusters, however, strong plasmon coupling occurs when the inter-particle gap distance becomes shorter than 10 nm, shifting the resonance to a near-infrared (NIR) region and lowering the absorption in the visible range (Barr et al., 2021; Liu et al., 2016; Liu and Lu, 2006; Mohsin and Salim, 2018; Tabor et al., 2009). Unlike other plasmonic applications harnessing plasmonic hot spots from nanogaps of AuNP clusters, for colorimetric LFI sensing, it is desired to construct AuNP clusters with a reproducible visible color by ensuring sufficient interparticle gap between AuNPs to avoid plasmon coupling. A few studies reported that the fabrication of AuNP-based clusters maintaining their red color for lateral flow assay (Hu et al., 2013; Li et al., 2020); however, they had a few limitations: i) complicated fabrication methods, ii) difficulty in conjugation with antibodies, and iii) relatively low sensitivity despite high absorbance of the AuNP-based clusters, which have limited the application of AuNP-based clusters for conventional LFIs.

Herein, we developed plasmon color-preserved (PLASCOP) AuNP clusters using streptavidin- and biotinylated antibody-adsorbed AuNPs to ensure an interparticle distance of ~15 nm; this preserves the plasmonic color of individual AuNPs after clustering (Scheme 1). The streptavidin (StA)-conjugated AuNP was used as the core; it was surrounded by biotinylated antibody (b-Ab)-conjugated AuNPs, bound through streptavidin-biotin interaction. Our PLASCOP AuNP cluster has four principal advantages: i) the use of StA (~5 nm) and b-Ab (~10 nm) enables maintaining enough interparticle gap for commercially available AuNPs, to prevent plasmonic coupling; ii) b-Ab, used as a linker for the cluster, functions as a bioreceptor for target detection, thereby alleviating the need for an additional step for antibody conjugation after cluster fabrication; iii) the cluster increases sensitivity, and the fabrication is easy, simple, and highly reproducible, because all the techniques are the gold standard methods for LFIs and the materials used for the fabrication are commercially available; and iv) this method can be applied to any AuNP-based conventional LFIs by changing the antibodies.

To demonstrate the potential of PLASCOP AuNP clusters, they have been incorporated within an LFI for the detection of SARS-CoV-2 exhibiting a significant improvement in sensitivity (compared to single AuNPs). In the context of the current pandemic and the detection of SARS CoV-2, early disease detection is essential for effective contact tracing (Kretzschmar et al., 2020). The utilization of LFI-based self-testing kits with improved sensitivity (i.e., incorporating novel PLASCOP AuNP clusters as proposed herein) could ameliorate the false negative rate associated with conventional LFI testing, particularly when such test kits are used during the early or late stages of infection (i.e., when the viral load is low) (Griffin, 2021).

2. Results and discussion

2.1. Plasmon color-preserved (PLASCOP) gold nanoparticle (AuNP) clusters

A key consideration for designing PLASCOP AuNP clusters is to form sufficient interparticle gaps to prevent the plasmon coupling between AuNPs. The optimal interparticle distance could vary depending on the size of AuNPs (Barr et al., 2021; Mohsin and Salim, 2018; Tabor et al., 2009). In general, the bigger AuNPs, the larger interparticle distance was required for the preservation of plasmonic properties (Barr et al., 2021). In the case of 40 nm AuNPs, which are commonly used in AuNP-based immunoassays, 10–20 nm gaps between AuNPs are regarded as sufficient, since the electromagnetic field weakens dramatically beyond 10 nm from the surface (Barr et al., 2021; Mohsin and Salim, 2018; Tabor et al., 2009). Thus, to fabricate PLASCOP AuNP clusters, we selected biotinylated antibodies and streptavidin (StA) in order to ensure sufficient interparticle distance, since in general, the sizes of the antibody and StA are approximately 10 nm and 5 nm, respectively (Kuzuya et al., 2008; Reth, 2013).

In PLASCOP AuNP clusters, we used streptavidin-coated AuNPs (AuNPs/StA) as a core and AuNPs conjugated with biotinylated antibodies (AuNPs/b-Ab) as satellites. This configuration ensures sufficient physical gaps between AuNPs and has antibodies exposed to the outer surface of clusters for immunoassays. We used AuNPs/StA and AuNPs/b-Ab at a ratio of 1:3 to enable the encapsulation of AuNPs/StA by AuNPs/b-Ab, while minimizing excess AuNPs/StA or AuNPs/b-Ab after clustering. We screened clusters fabricated at ratios of 1:3, 1:1, 3:1, etc (Data are not shown in this article.), and the 1:3 conjugate exhibited good sensitivity. It is possible that this ratio is not optimal; however, it provided consistent and promising results with good sensitivity. There is scope for further optimizing the ratio by altering the sizes of the core and satellite AuNPs, pore size of the membrane, and composition of running buffer. This should be explored in future studies.

We used transmission electron microscopy (TEM) to confirm the structure of PLASCOP AuNP clusters (Fig. 1). Using 40 nm AuNPs/StA

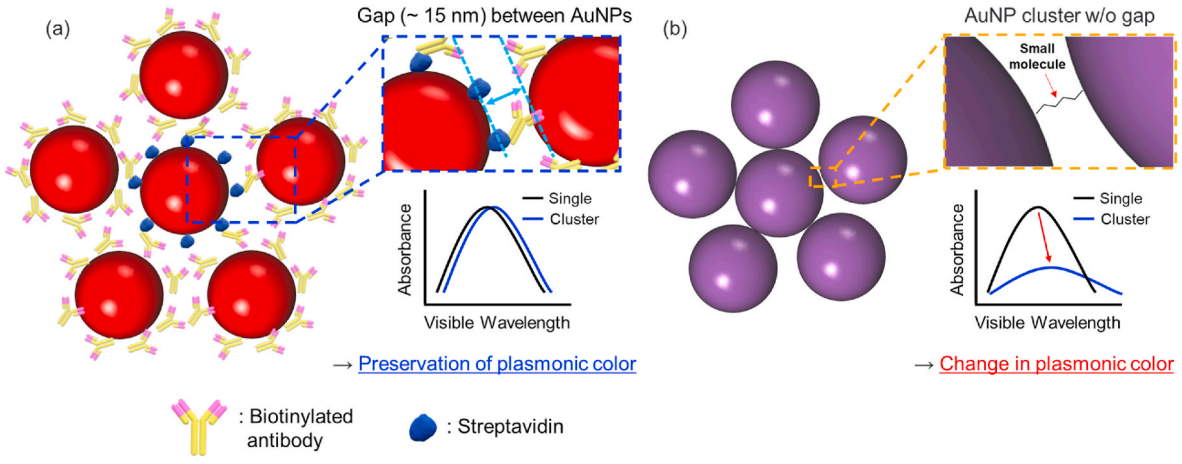

Scheme 1. Schematic illustration of AuNP-based clusters and their absorption properties when using (a) proteins such as streptavidin and biotinylated antibodies as proposed herein, and (b) a typical small molecule.

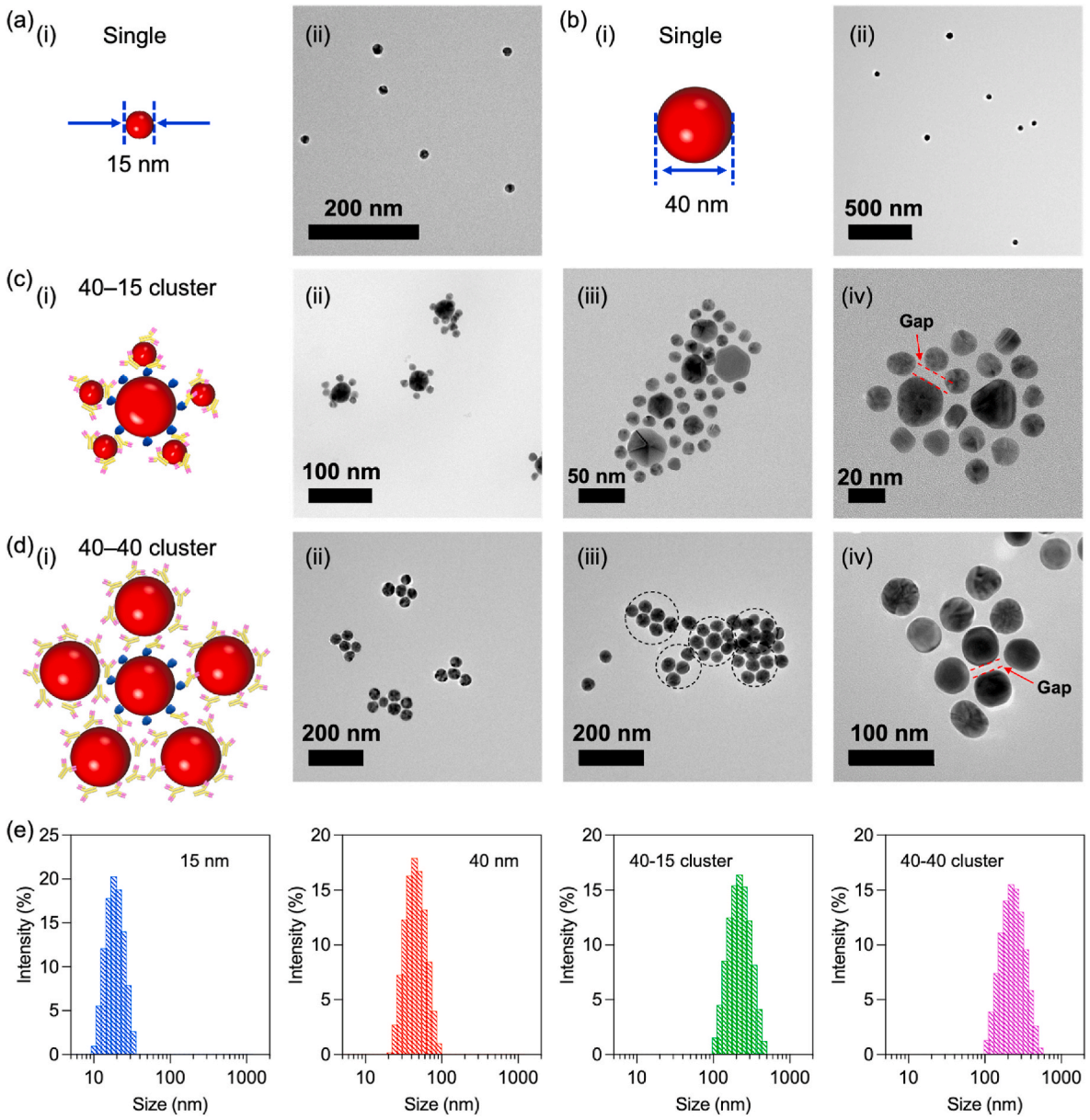

Fig. 1. Schematic illustrations (i) and TEM images (ii, iii, iv) of (a) 15 nm and (b) 40 nm individual AuNPs; (c) 40 nm AuNPs/StA and 15 nm AuNPs/b-Ab conjugate-based PLASCOP AuNP clusters; and (d) 40 nm AuNPs/StA and 40 nm AuNPs/b-Ab conjugate-based PLASCOP AuNP clusters. (e) Hydrodynamic diameters of 15 nm and 40 nm single AuNPs and 40-15 and 40-40 AuNP clusters.

and 15 nm AuNPs/b-Ab (Fig. 1a and b), we successfully made PLASCOP AuNP clusters (40-15 clusters; Fig. 1c). On average, seven numbers of 15 nm AuNPs/b-Ab were bound to single 40 nm AuNPs/StA (Fig. 1c (ii)). In some cases, multiple AuNPs/StA-based clusters were formed, leading to form larger PLASCOP clusters, as shown in Fig. 1c (iii). Interparticle gaps can also be clearly seen in Fig. 1c (iv). It should be noted that it is difficult to measure the exact interparticle distance between AuNPs from TEM images because TEM is only capable of projecting two-dimensional images. In other words, the interparticle distance between the AuNPs is not exactly measurable unless all of the AuNPs at the clusters are located on the same two-dimensional plane.

We also made another PLASCOP AuNPs using 40 nm AuNPs/StA and 40 nm AuNPs/b-Ab (40-40 clusters; Fig. 1d). Unlike the 40-15 clusters (Fig. 1c), differentiation of the core/shell structure in clusters with 40 nm AuNPs/StA and 40 nm AuNPs/b-Ab was more difficult, as they are the same size. Nevertheless, similar shapes were observed for 40-40 clusters (Fig. 1d (ii &iii)), compared to that of 40-15 clusters (Fig. 1 (ii & iii)). Similar to 40-15 clusters, some of the 40-40 clusters were formed based on single AuNPs/StA (Fig. 1d(ii)) and some others were formed based on multiple AuNPs/StA (Fig. 1d (iii)). In addition, interparticle gaps can be clearly seen in Fig. 1 (iv). Hence, the PLASCOP AuNP clusters were successfully fabricated in terms of (i) core and satellite formations based on AuNPs/StA and AuNPs/b-Ab, respectively; and (ii) interparticle gap formations (approximately 15 nm) using antibodies and StA.

The hydrodynamic diameters of the 40-15 and 40-40 clusters were around 229 nm and 244 nm, respectively, and those of the commercial 15 nm and 40 nm AuNPs were 18 nm and 42 nm, respectively (Fig. 1e).

We next characterized the optical properties of PLASCOP AuNP clusters (Figs. 2 and S1). The forty nanometers single AuNPs showed absorption peaks (λ_{max}) at 529 nm; 531 nm for 40 nm AuNPs/StA, and; 531 nm for 40 nm AuNPs/b-Ab. PLASCOP AuNPs clusters (40-40 clusters) showed λ_{max} at 532 nm, only shifted by 1 nm from the core AuNPs/StA (Fig. 2a). 40-15 clusters also showed no plasmon coupling after

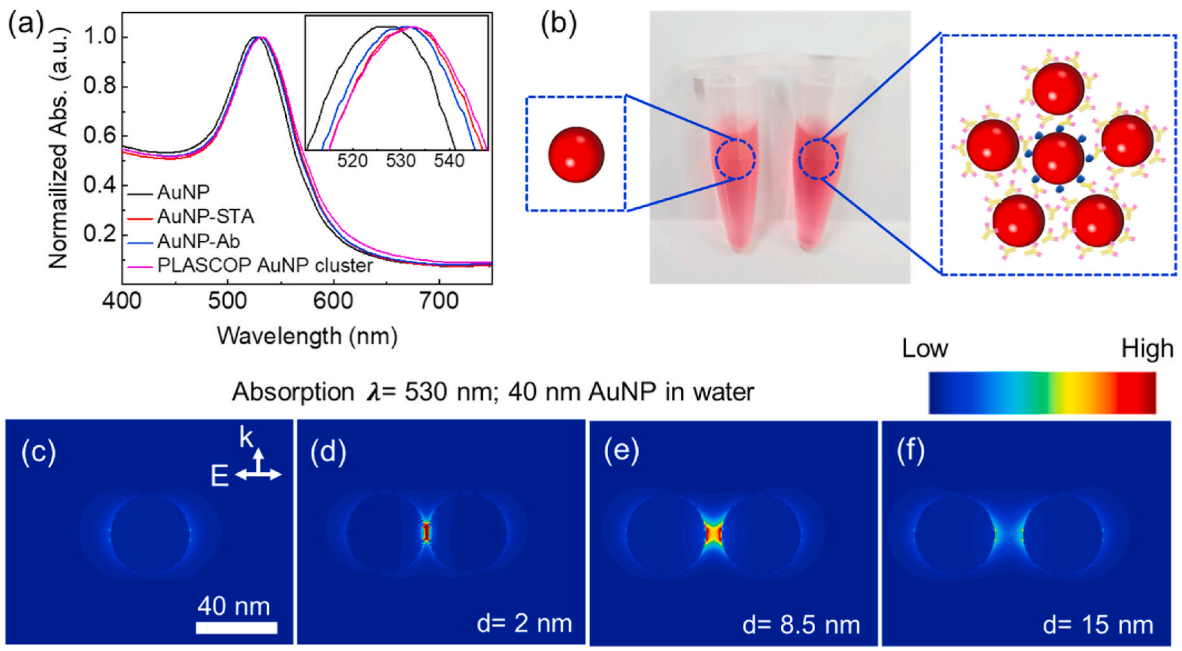

Fig. 2. (a) Absorption spectra of bare 40 nm AuNPs, 40 nm AuNPs/StA, 40 nm AuNPs/b-Ab, and 40-40 clusters (Maximum LSPR peak intensity values of each sample were normalized to a value of 1.0.). (b) A photograph of 40 nm AuNPs and 40-40 nm cluster solutions in tubes. (c–f) FDTD simulation results include: (c) single AuNP, and dual AuNPs with interparticle gaps: (d) 2 nm, (e) 8.5 nm, and (f) 15 nm at a wavelength of 530 nm in water. The size of the AuNPs was 40 nm. The wave vectors of K and E represent the incident direction of the monochromatic light and the polarization direction, respectively.

clustering (Fig. S1). As a result, PLASCOP AuNP clusters maintain the same color as single AuNPs (Fig. 2b). To better understand the optical properties, we utilized electrodynamic computation with the finite-difference time-domain (FDTD) method to simulate electric field distribution of single and dual AuNPs (Fig. 2c–f). The FDTD simulation shows weak plasmon coupling between AuNPs when the interparticle gap size becomes 15 nm. This aligns with the expected gap distance (~15 nm) with StA and b-Ab linkers, which avoids the plasmon coupling phenomenon and maintains the plasmonic property of individual AuNPs in the PLASCOP AuNP clusters.

To demonstrate the gap size effect, we made AuNP clusters using a small molecule, melamine, which is known to induce AuNP clusters with a small gap size of <2 nm (Ma et al., 2014; Siddiquee et al., 2021). As expected absorbance of melamine-induced AuNP clusters decreased in LSPR peak intensity at 530 nm (visible wavelength) and increased in the intensity for wavelengths >700 nm (near-infrared (NIR) region) (Fig. S3a), resulting in a color change from red to pale purple (Fig. S3b). In Fig. S4, the TEM images show AuNP clusters with no distinct interparticle gap between the AuNPs. Consequently, AuNP clusters with narrow interparticle gaps are not suitable for colorimetric immunoassays.

2.2. Detection of SARS-CoV-2 nucleocapsid proteins using PLASCOP AuNP clusters in LFI

Severe acute respiratory syndrome-associated coronavirus (SARS-CoV, 2002; China) (Zhong et al., 2003), Middle East respiratory syndrome coronavirus (MERS-CoV, 2012; Saudi Arabia) (Alyami et al., 2020), and severe acute respiratory syndrome coronavirus 2 (SARS-CoV-2, 2019, China) have emerged over time and triggered global pandemics (Lai et al., 2020). In particular, SARS-CoV-2 is very contagious with a much higher transmission rate and asymptomatic infection (Chan et al., 2020; World Health Organization (WHO)), causing over 230 million confirmed cases and 4.7 million deaths as reported by the World Health Organization at the time of writing (World Health Organization (WHO)). As the vaccination rate has increased, the number of infected cases were expected to decrease; however, the confirmed cases of COVID-19 have shown signs of increasing and this trend is associated with the emergence of the delta variant (2020, India) (Kupferschmidt and Wadman 2021; O'Dowd 2021; World Health Organization (WHO)). In this difficult situation, LFI-based diagnostic kits that can be easily used by patients or the general public for screening have emerged as an important solution; however, the disadvantages of low sensitivity and insufficient quantitation capability still remain to be solved. Thus, the novel PLASCOP AuNP clusters (as discussed in the previous section) were incorporated within LFI sensors for the colorimetric detection of the SARS-CoV-2 nucleocapsid protein, in order to demonstrate the extent to which LFI sensitivity can be enhanced.

The PLASCOP AuNP clusters were applied to LFI for the detection of SAVS-CoV-2 nucleocapsid proteins. We validated the diffusion property of the synthesized clusters through the membrane under lateral flow (Fig. S5). All synthesized clusters were prepared in Tris (0.1 M, pH 8) with 1% Triton X-100, and applied to the membrane. All the clusters exhibited diffusion through the membrane without any nonspecific sedimentation. There was no significant difference between the colorimetric images from samples using our clusters and those prepared with the individual 40-nm AuNPs. We validated the activities of antibodies before and after biotinylation. When the antibodies were applied to detect SARS-CoV-2 nucleocapsid proteins on LFIs, there was no difference in sensitivity (Fig. S6). This confirmed that the activity of the antibodies was maintained even after biotinylation.

We tested the detection sensitivity of PLASCOP AuNP clusters (40-15 and 40-40 clusters) in comparison to two different AuNPs sizes (15 nm and 40 nm) on LFI strips. The colorimetric images were captured using a ChemiDoc MP system after applying SARS-CoV-2 nucleocapsid proteins to LFI strips (Fig. 3a). The images were analyzed using Image Lab software (6.0.1) to quantify the colorimetric signal intensities on the strips (Fig. 3b). In the case of PLASCOP AuNP clusters (40-15 and 40-40 clusters), the color of both test and control lines on the strips is red (Figs. S7a and S7b), which is the same as that with individual 40 nm AuNPs (Fig. S7c). From the colorimetric signal intensities, a calibration plot of intensity versus SARS-CoV-2 nucleocapsid proteins concentration (from 0.01 to 1000 ng mL^{-1}) was obtained based on a sigmoidal function. All the individual AuNPs and PLASCOP AuNP clusters showed

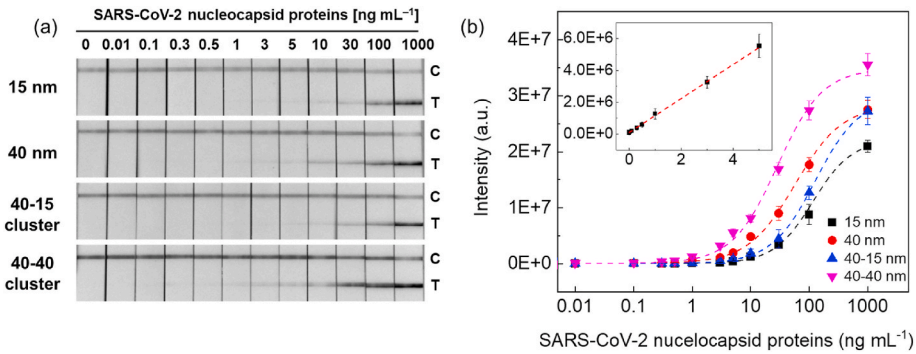

Fig. 3. (a) Colorimetric images after detection of SARS-CoV-2 nucleocapsid proteins using individual AuNPs (15 nm and 40 nm) and PLASCOP AuNP clusters (40-15 and 40-40 clusters) within the concentration range of 0–1000 ng mL^{-1}. C and T denote control line and test line, respectively. (b) Comparison of colorimetric intensities of test lines on each paper strip shown in Fig. 3(a). The colorimetric intensities were obtained from a ChemiDoc MP system and Image Lab software (6.0.1).

increasing colorimetric intensities with increase in SARS-CoV-2 nucleocapsid protein concentration. The LFI sensing with PLASCOP AuNP clusters showed significantly improved detection ranges was from 30 pg mL^{-1} to 1,000 ng mL^{-1} while the detection ranges of individual 15 nm AuNPs, 40 nm AuNPs, and 40-15 clusters were from 1 ng mL^{-1} to 1,000 ng mL^{-1}. Moreover, the limits of detection (LODs) of 15 nm AuNPs, 40 nm AuNPs, 40-15 clusters, and 40-40 clusters were calculated as 0.910, 0.226, 0.551, and 0.038 ng mL^{-1}, respectively (based on S/N = 5). The LOD was calculated using Eq. (1):

$$LOD = \frac{3\sigma}{S} \quad (1)$$

where σ and S are the standard deviation of the response and the slope of the calibration curve, respectively.

Collectively, the results demonstrate that the PLASCOP AuNP clusters show high sensitivity in the immunoassay. Table 1 summarizes the sensing performances of the individual AuNPs and PLASCOP AuNP clusters for the detection of SARS-CoV-2 nucleocapsid proteins. We speculate that there are two main reasons for the higher sensitivity of PLASCOP AuNP (40-40) clusters compared to individual AuNPs. First, the clusters can react with more antigens because more antibodies are exposed on the surface than that in single particles. Second, a single AuNP/detection antibody conjugate is immobilized on capture antibody attached to a membrane via a single antigen in individual AuNP-based conjugates. However, in the case of the cluster-based conjugates, a group of AuNPs is immobilized on the capture antibody via a single antigen. There was one exception; the sensitivity of the 40-15 cluster was lower than that of the individual 40-nm AuNP but higher than that of the 20-nm AuNP. This possibly indicates the lower sensitivity of the 40-15 nm AuNP clusters compared to that of the single 40 nm AuNPs. This could be due to the lower density of the antibody attachment on the 15 nm AuNPs in the 40-15 cluster and the low diffusivity.

2.3. Specificity test using other nucleocapsid proteins

We next tested the specificity of the PLASCOP AuNP cluster-based LFI sensors by detecting various nucleocapsid proteins (10 ng mL^{-1}) from the following: SARS-CoV-2, influenza A, influenza B, Middle East respiratory syndrome coronavirus (MERS-CoV), and human coronavirus 229E (HCoV-229E). Characterization methods were the same as those described above; briefly, colorimetric images were captured and analyzed using a ChemiDoc MP system and Image Lab software (6.0.1). Specificity test results revealed that the PLASCOP AuNP cluster-based LFI sensors could only detect SARS-CoV-2 nucleocapsid proteins, as shown in Fig. 4. Thus, our PLASCOP AuNP cluster-based LFI sensors show promising selectivity platform for the detection of SARS-CoV-2 nucleocapsid proteins.

Table 1
Comparison of the detection performance of individual AuNPs and PLASCOP AuNP clusters toward SARS-CoV-2 nucleocapsid proteins.

Labels		Detection range (ng mL^{-1})	R^2	LOD (ng mL^{-1})
Individual AuNPs	15	1 to 1,000	0.993	0.910
	40	1 to 1,000	0.964	0.226
Clusters	40–15	1 to 1,000	0.993	0.550
	40–40	0.3 to 1,000	0.974	0.038

2.4. Detection of the SARS CoV-2 virus particles from saliva samples

We next tested the sensitivity of the PLASCOP AuNP cluster-based LFI sensors with virus-free human saliva samples spiked with SARS-CoV-2 particles. The samples were prepared by spiking known amounts of virus particles at concentrations ranging from 12 to 355 $TCID_{50}$ mL^{-1} (50 percent tissue culture infectious doses per milliliter). The virus-spiked human saliva was directly applied to the LFI sensors, and after immunoassay, colorimetric images of the LFI sensors were captured and analyzed using a ChemiDoc MP system and Image Lab software (6.0.1). The results confirmed that the PLASCOP AuNP cluster-based LFI sensors could detect SARS-CoV-2 virus particles in a complex saliva matrix with a detection limit corresponding to 54 $TCID_{50}$ mL^{-1} (Fig. 5). The LOD was calculated using Eq. (1) given above. In addition, we have summarized and compared the performance and features of our PLASCOP AuNP cluster-based LFI sensors with previous studies (Table 2). In addition, we also compared the sensitivity with commercialized COVID-19 rapid test kits, obtained from two companies (Fig. S8). Our cluster-based LFI exhibits improved performance compared to those from earlier studies. It exhibits similar or higher sensitivity compared to that of commercial test kits which are sold worldwide. The sensitivity of LFIs is generally determined using an optical probe, the affinity of an antibody pair, composition of an assay buffer, or the pore size of a membrane. The commercial test kits are well-optimized. We focused on developing a highly sensitive optical probe; therefore, there is excellent potential for further improvement of the sensitivity of our PLASCOP clusters-based LFI platform.

3. Conclusions

In this study, we demonstrated the plasmon color-preserved (PLASCOP) gold nanoparticle (AuNP) clusters using a simple and reproducible method. This could be easily and widely applied to colorimetric immunosensors to enhance sensitivity. The preservation of the plasmonic color after AuNP clustering was ensured using streptavidin (StA)-loaded AuNPs and biotinylated antibody (b-Ab)-loaded AuNPs. These had sufficient interparticle distance between the AuNPs, theoretically about 15 nm. Structurally, the AuNPs/StA were surrounded by several

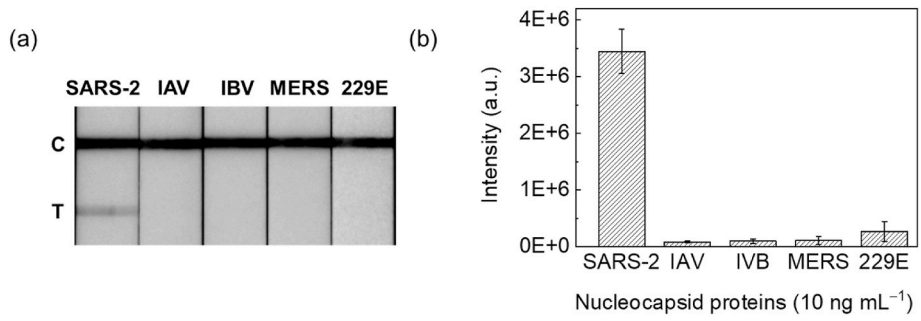

Fig. 4. Specificity tests using 40-40 clusters on LFI sensors. (a) Colorimetric images of each strip detecting nucleocapsid proteins (10 ng mL^{-1}) from various viruses including SARS-CoV-2, influenza A, influenza B, MERS-CoV, and HCoV-229E. C and T denote the control line and test line, respectively. (b) The signal intensity of each strip. Error bars indicate the standard deviation from three independent experiments.

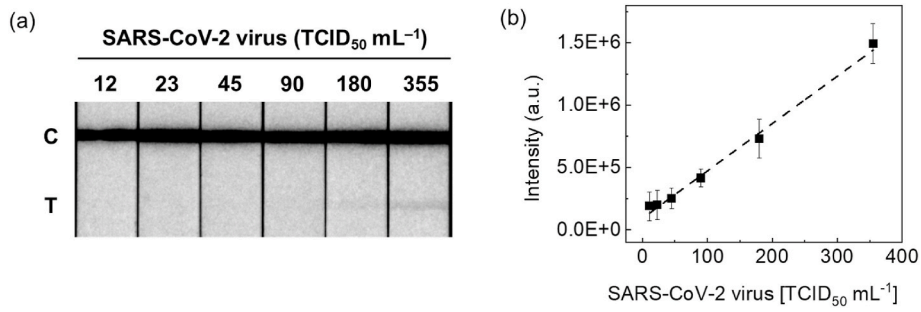

Fig. 5. Virus sample detection using 40-40 clusters on LFI sensors. Colorimetric (a) images and (b) intensities of the strips used for SARS-CoV-2 virus particle-spiked human saliva samples within the concentration range of 12–355 $TCID_{50}$ mL^{-1}. C and T denote the control line and test line, respectively.

Table 2
Comparison of the specificities of the PLASCOP AuNP cluster-based LFI sensor with previously developed lateral flow immunoassay (LFI).

No.	Probe	Limit of detection (LOD)	Assay time	Detection method	Ref.
1	Gold nanoparticles	250 pg mL^{-1}	15 min	–	Mertens et al. (2020)
2	Latex beads	650 pg mL^{-1}	30 min	Optical reader	Grant et al. (2020)
3	Fluorescent microparticles	–	10 min	Fluorescence analyzer	Diao et al. (2021)
4	Fluorescent microsphere	100 ng mL^{-1}	15 min	UV-LED/detector	Zhang et al. (2020a)
This study	PLASCOP AuNP clusters	38 pg mL^{-1}	10 min	Optical reader	–

AuNPs/b-Ab via streptavidin-biotin interaction, at an AuNPs/b-Ab: AuNPs/StA ratio of 3:1. The antibodies were naturally exposed to the surrounding media and could readily bind to target molecules. The number of AuNPs constituting the PLASCOP AuNP clusters ranged from a few to several tens, which was observed by TEM.

As a model study, the novel PLASCOP AuNP clusters were used to detect SARS-CoV-2 nucleocapsid proteins; in particular, the 40-40 clusters showed the highest performance with an LOD of 0.038 ng mL^{-1}, and detection range from 300 pg mL^{-1} to 1,000 ng mL^{-1}. The LOD of the 40-40 clusters was, at least, 5.9 and 23.9 times lower than that of individual 40 nm and 15 nm AuNPs conjugate, respectively. We compared our relatively simple platform with commercially available COVID-19 test kits; it showed similar or higher sensitivity in each case. It is vital that the test kits are sensitive to detect low viral loads, which is essential for detecting the early and late stages of infection. The sensitivity of our approach, using PLASCOP AuNP clusters for LFI, could be enhanced further by i) controlling the size and the number of AuNPs within the PLASCOP AuNP clusters, ii) using membranes with different pore sizes, and iii) optimizing the composition of the running buffer.

Our PLASCOP AuNP clusters could selectively detect the SARS-CoV-2 nucleocapsid protein relative to those of influenza A and B viruses, MERS-CoV, and HCoV-229E. The PLASCOP AuNP clusters were further applied to detect SARS-CoV-2 in virus-spiked human saliva with a concentration range of 12–355 $TCID_{50}$ mL^{-1}, and the LOD was found to be 54 $TCID_{50}$ mL^{-1}. Such an approach that uses PLASCOP AuNP clusters could improve sensitivity further by controlling the number of AuNPs contained within the PLASCOP AuNP clusters. Therefore, we can conclude that the PLASCOP AuNP clusters show exceptional potential as highly sensitive and general-purpose colorimetric signal reporters, which can be incorporated within LFIs to enable earlier diagnosis of a variety of diseases not limited to SARS-CoV-2 as demonstrated herein.

Authorship contribution statement

Hyun-Kyung Oh and Kihyeun Kim contributed equally to this work. All authors contributed to the writing of the manuscript and have given their approval for the final version of the manuscript.

CRediT authorship contribution statement

Hyun-Kyung Oh: Methodology, Validation, Formal analysis, Data curation, Writing – original draft, Visualization. **Kihyeun Kim:** Methodology, Formal analysis, Data curation, Writing – original draft, Visualization. **Jinhee Park:** Validation. **Hyungsoon Im:** Writing – review & editing. **Simon Maher:** Writing – review & editing. **Min-Gon Kim:** Conceptualization, Investigation, Resources, Supervision, Project administration, Funding acquisition.

Declaration of competing interest

The authors declare that they have no known competing financial interests or personal relationships that could have appeared to influence the work reported in this paper.

Acknowledgements

This work was financially supported by a National Research Foundation grant funded by the Ministry of Science, ICT, and Future Planning as the MidCareer Researcher Program (NRF2021R1A2B5B3001417); a BioNano Health Guard Research Center funded by the Ministry of Science, ICT, and Future Planning of Korea as the Global Frontier Project (H-GUARD_NRF-2019M3A6B2060097); Gwangju Institute of Science and Technology (GIST) as the GIST Young Scientist Research Project in 2021; a Korea Innovation Foundation funded by the Ministry of Science and ICT as the Technology commercialization capability enhancement project (2020-GJ-RD-0170); and UKRI, Engineering and Physical Sciences Research Council (EP/V001019/1).

Appendix A. Supplementary data

Supplementary data to this article can be found online at https://doi.org/10.1016/j.bios.2022.114094.

References

Alyami, M.H., Alyami, H.S., Warraich, A., 2020. Middle East Respiratory Syndrome (MERS) and novel coronavirus disease-2019 (COVID-19): from causes to preventions in Saudi Arabia. Saudi Pharmaceut. J. 28 (11), 1481–1491.

Barr, J.W., Gomrok, S., Chaffin, E., Huang, X., Wang, Y., 2021. Insight on the coupling of plasmonic nanoparticles from near-field spectra determined via discrete dipole approximations. J Phys Chem C Nanomater Interfaces 125 (9), 5260–5268.

Chan, J.F.-W., Yuan, S., Kok, K.-H., To, K.K.-W., Chu, H., Yang, J., Xing, F., Liu, J., Yip, C. C.-Y., Poon, R.W.-S., Tsoi, H.-W., Lo, S.K.-F., Chan, K.-H., Poon, V.K.-M., Chan, W.-M., Ip, J.D., Cai, J.-P., Cheng, V.C.-C., Chen, H., Hui, C.K.-M., Yuen, K.-Y., 2020. A familial cluster of pneumonia associated with the 2019 novel coronavirus indicating person-to-person transmission: a study of a family cluster. Lancet 395 (10223), 514–523.

Chen, X., Leng, Y., Hao, L., Duan, H., Yuan, J., Zhang, W., Huang, X., Xiong, Y., 2020. Self-assembled colloidal gold superparticles to enhance the sensitivity of lateral flow immunoassays with sandwich format. Theranostics 10 (8), 3737–3748.

Diao, B., Wen, K., Zhang, J., Chen, J., Han, C., Chen, Y., Wang, S., Deng, G., Zhou, H., Wu, Y., 2021. Accuracy of a nucleocapsid protein antigen rapid test in the diagnosis of SARS-CoV-2 infection. Clin. Microbiol. Infect. 27 (2), 289 e281-289 e284.

Diaz-Gonzalez, M., de la Escosura-Muniz, A., 2021. Strip modification and alternative architectures for signal amplification in nanoparticle-based lateral flow assays. Anal. Bioanal. Chem. 413 (16), 4111–4117.

Drain, P.K., Hyle, E.P., Noubary, F., Freedberg, K.A., Wilson, D., Bishai, W.R., Rodriguez, W., Bassett, I.V., 2014. Diagnostic point-of-care tests in resource-limited settings. Lancet Infect. Dis. 14 (3), 239–249.

Grant, B.D., Anderson, C.E., Williford, J.R., Alonzo, L.F., Glukhova, V.A., Boyle, D.S., Weigl, B.H., Nichols, K.P., 2020. SARS-CoV-2 coronavirus nucleocapsid antigen-detecting half-strip lateral flow assay toward the development of point of care tests using commercially available reagents. Anal. Chem. 92 (16), 11305–11309.

Griffin, S., 2021. Covid-19: lateral flow tests are better at identifying people with symptoms, finds Cochrane review. BMJ 372, n823.

Hu, J., Wang, L., Li, F., Han, Y.L., Lin, M., Lu, T.J., Xu, F., 2013. Oligonucleotide-linked gold nanoparticle aggregates for enhanced sensitivity in lateral flow assays. Lab Chip 13 (22), 4352–4357.

Khlebtsov, B.N., Tumskiy, R.S., Burov, A.M., Pylaev, T.E., Khlebtsov, N.G., 2019. Quantifying the numbers of gold nanoparticles in the test zone of lateral flow immunoassay strips. ACS Appl. Nano Mater. 2 (8), 5020–5028.

Koczula, K.M., Gallotta, A., 2016. Lateral flow assays. Essays Biochem. 60 (1), 111–120.

Kretzschmar, M.E., Rozhnova, G., Bootsma, M.C.J., van Boven, M., van de Wijgert, J.H.H. M., Bonten, M.J.M., 2020. Impact of delays on effectiveness of contact tracing strategies for COVID-19: a modelling study. Lancet Public Health 5 (8), e452–e459.

Kupferschmidt, K., Wadman, M., 2021. Delta Variant Triggers New Phase in the Pandemic. American Association for the Advancement of Science.

Kuzuya, A., Numajiri, K., Kimura, M., Komiyama, M., 2008. Single-molecule accommodation of streptavidin in nanometer-scale wells formed in DNA nanostructures. Nucleic Acids Symp. Ser. (52), 681–682.

Lai, C.C., Shih, T.P., Ko, W.C., Tang, H.J., Hsueh, P.R., 2020. Severe acute respiratory syndrome coronavirus 2 (SARS-CoV-2) and coronavirus disease-2019 (COVID-19): the epidemic and the challenges. Int. J. Antimicrob. Agents 55 (3), 105924.

Li, J., Duan, H., Xu, P., Huang, X., Xiong, Y., 2016. Effect of different-sized spherical gold nanoparticles grown layer by layer on the sensitivity of an immunochromatographic assay. RSC Adv. 6 (31), 26178–26185.

Li, Y., Chen, X., Yuan, J., Leng, Y., Lai, W., Huang, X., Xiong, Y., 2020. Integrated gold superparticles into lateral flow immunoassays for the rapid and sensitive detection of Escherichia coli O157:H7 in milk. J. Dairy Sci. 103 (8), 6940–6949.

Liu, G., Wang, S., Yang, X., Li, T., She, Y., Wang, J., Zou, P., Jin, F., Jin, M., Shao, H., 2016. Colorimetric sensing of atrazine in rice samples using cysteamine functionalized gold nanoparticles after solid phase extraction. Anal. Methods 8 (1), 52–56.

Liu, J., Lu, Y., 2006. Preparation of aptamer-linked gold nanoparticle purple aggregates for colorimetric sensing of analytes. Nat. Protoc. 1 (1), 246–252.

Ma, H., Wu, B., Huang, C., Jia, N., 2014. One-step highly sensitive detection of melamine using gold nanoparticle-based dynamic light scattering. Anal. Methods 6 (1), 67–72.

Mertens, P., De Vos, N., Martiny, D., Jassoy, C., Mirazimi, A., Cuypers, L., Van den Wijngaert, S., Monteil, V., Melin, P., Stoffels, K., Yin, N., Mileto, D., Delaunoy, S., Magein, H., Lagrou, K., Bouzet, J., Serrano, G., Wautier, M., Leclipteux, T., Van Ranst, M., Vandenberg, O., Group, L.-U.S.-C.-W.D., 2020. Development and potential usefulness of the COVID-19 Ag respi-strip diagnostic assay in a pandemic context. Front. Med. 7, 225.

Mohsin, A.S.M., Salim, M.B., 2018. Probing the plasmon coupling, quantum yield, and effects of tip geometry of gold nanoparticle using analytical models and FDTD simulation. IEEE Photonics J. 10 (3), 1–10.

O'Dowd, A., 2021. Covid-19: cases of delta variant rise by 79%, but rate of growth slows. BMJ 373, n1596.

Parolo, C., Sena-Torralba, A., Bergua, J.F., Calucho, E., Fuentes-Chust, C., Hu, L., Rivas, L., Alvarez-Diduk, R., Nguyen, E.P., Cinti, S., Quesada-Gonzalez, D., Merkoci, A., 2020. Tutorial: design and fabrication of nanoparticle-based lateral-flow immunoassays. Nat. Protoc. 15 (12), 3788–3816.

Price, C.P., 2001. Point of care testing. BMJ 322 (7297), 1285–1288.

Reth, M., 2013. Matching cellular dimensions with molecular sizes. Nat. Immunol. 14 (8), 765–767.

Sajid, M., Kawde, A.-N., Daud, M., 2015. Designs, formats and applications of lateral flow assay: a literature review. J. Saudi Chem. Soc. 19 (6), 689–705.

Shen, Y., Shen, G., 2019. Signal-enhanced lateral flow immunoassay with dual gold nanoparticle conjugates for the detection of hepatitis B surface antigen. ACS Omega 4 (3), 5083–5087.

Shirshahi, V., Liu, G., 2021. Enhancing the analytical performance of paper lateral flow assays: from chemistry to engineering. Trac. Trends Anal. Chem. 136.

Siddiquee, S., Saallah, S., Bohari, N.A., Ringgit, G., Roslan, J., Naher, L., Hasan Nudin, N. F., 2021. Visual and optical absorbance detection of melamine in milk by melamine-induced aggregation of gold nanoparticles. Nanomaterials 11 (5).

Tabor, C., Murali, R., Mahmoud, M., El-Sayed, M.A., 2009. On the use of plasmonic nanoparticle pairs as a plasmon ruler: the dependence of the near-field dipole plasmon coupling on nanoparticle size and shape. J. Phys. Chem. 113 (10), 1946–1953.

Vashist, S.K., Luppa, P.B., Yeo, L.Y., Ozcan, A., Luong, J.H.T., 2015. Emerging technologies for next-generation point-of-care testing. Trends Biotechnol. 33 (11), 692–705.

Wang, K., Qin, W., Hou, Y., Xiao, K., Yan, W., 2016. The application of lateral flow immunoassay in point of care testing: a review. Nano Biomed. Eng. 8 (3).

Warsinke, A., 2009. Point-of-care testing of proteins. Anal. Bioanal. Chem. 393 (5), 1393–1405.

Zhang, C., Zhou, L., Du, K., Zhang, Y., Wang, J., Chen, L., Lyu, Y., Li, J., Liu, H., Huo, J., Li, F., Wang, J., Sang, P., Lin, S., Xiao, Y., Zhang, K., He, K., 2020a. Foundation and clinical evaluation of a new method for detecting SARS-CoV-2 antigen by fluorescent microsphere immunochromatography. Front Cell Infect Microbiol 10, 553837.

Zhang, L., Mazouzi, Y., Salmain, M., Liedberg, B., Boujday, S., 2020b. Antibody-gold nanoparticle bioconjugates for biosensors: synthesis, characterization and selected applications. Biosens. Bioelectron. 165, 112370.

Zhong, N.S., Zheng, B.J., Li, Y.M., Poon, L.L.M., Xie, Z.H., Chan, K.H., Li, P.H., Tan, S.Y., Chang, Q., Xie, J.P., Liu, X.Q., Xu, J., Li, D.X., Yuen, K.Y., Peiris, J.S.M., Guan, Y., 2003. Epidemiology and cause of severe acute respiratory syndrome (SARS) in Guangdong, People's Republic of China, in February, 2003. Lancet 362 (9393), 1353–1358.

Zhou, W., Gao, X., Liu, D., Chen, X., 2015. Gold nanoparticles for in vitro diagnostics. Chem. Rev. 115 (19), 10575–10636.